Generation of Fast Neutral Beams by Ion Neutralization in High-Aspect-Ratio Holes: A Particle-in-Cell Simulation Study

Sang Ki Nam, Demetre J. Economou, and Vincent M. Donnelly

***Abstract*—In this paper, a particle-in-cell simulation of ion and neutral-beam extraction through a grid with high-aspect-ratio holes in contact with plasma was developed. Particular emphasis was placed on plasma molding over the holes, ion neutralization along the sidewall of the holes, and the energy and angular distributions of the residual ions and fast neutrals in the beam downstream of the holes. The target application was the generation of fast neutral beams for future charge-free microelectronics manufacturing. The energy and angular distributions of ions at different locations along the hole sidewall showed that ions which neutralize on the top section of the surface of the hole are "bad," in the sense that these ions yield divergent neutral beams of relatively low energy. Ions that neutralize along the bottom section of the hole sidewall are "good," in the sense that these ions yield neutral beams that are less divergent and retain more of the energy of the parent ions. A three-grid ion-extraction/neutralization system is proposed to increase the fraction of good ions and produce a higher quality neutral beam.**

***Index Terms*—Charge-free semiconductor manufacturing, energetic neutral beams, neutral-beam sources, particle-in-cell (PIC), plasma processing, simulation.**

I. Introduction

With each new generation of integrated circuits, the ability to form ever smaller features by plasma etching has become increasingly challenging, in large part, due to the differential charging resulting from ion and electron bombardment of the wafer [1]. Since ions coming out of a plasma are much more directional than electrons, microfeatures on the wafer surface tend to charge negatively along the sidewall and positively at the bottom. This differential charging can cause subsequent ions coming into the microfeature to deflect and their trajectories to bend to the point that these ions induce sidewall damage (e.g., notching, bowing, etc.). Charging may also be responsible for reactive-ion-etching lag and etch stop due to the reduction of the ion current and energy to the bottom of the microfeature as a function of depth [1], [2].

The adverse effects of charging could be eliminated by using energetic neutral beams (atoms or molecules), instead of ions, to give the directional component required for anisotropic etching. Moreover, this neutral-beam etching, neutral-beam processing in general, may be useful for other thin-film technologies, including deposition, oxidation [3], and even photolithography.

A fast [10–100 s of electronvolt (eV)] neutral beam may be created by extracting ions, which are generated in a high-density inductively coupled plasma, through a grounded metal grid with high-aspect-ratio holes [4], [5]. Ions suffer grazing-angle collisions with the inside surfaces of the holes, turning into neutrals. The plasma power controls the beam flux. A separate power supply connected to a "beam accelerator electrode" immersed in the plasma controls the plasma potential and, hence, the beam energy. Other techniques to generate fast neutral beams are also based on ion extraction from a plasma through a grid. Ions are subsequently neutralized either by charge exchange with a background gas [6] or by allowing the ions to reflect off of a conducting plate placed at an angle with respect to the substrate [7]–[9].

In any case, the flux, energy, and angular distributions of the extracted beam are of primary importance for applications such as etching and deposition used in microfabrication [10]. These beam properties can be critically affected by plasma molding over the grid holes [11]–[13]. Plasma molding refers to the ability of the plasma–sheath interface to "contour" along the topography of surface features in contact with the plasma. In the case of a plasma in contact with a grid, plasma molding depends primarily on the diameter of the grid holes D as compared to the plasma–sheath thickness L_{sh}. When $L_{sh} \gg D$, the plasma–sheath interface (meniscus) is essentially planar as if the holes were not there (e.g., a solid wall). In the other extreme, $L_{sh} \ll D$, the plasma "leaks" through the holes. In the intermediate case, $L_{sh} \sim D$, the plasma–sheath meniscus "bends" gently over the holes [11]. The resulting beam should be directional (assuming no collisions in the sheath) when $L_{sh} \gg D$ and divergent when $L_{sh} \ll D$. On the other hand, the energy of the beam will depend on the potential difference between the plasma and the extraction grid.

Manuscript received February 6, 2007; revised June 30, 2007. This work was supported in part by the State of Texas (Texas Advanced Research and Texas Advanced Technology Programs) and in part by the National Science Foundation (MII-0303790).

S. K. Nam was with the Plasma Processing Laboratory, Department of Chemical and Biomolecular Engineering, University of Houston, Houston, TX 77204-4004 USA. He is now with the Department of Nuclear Engineering, University of California, Berkeley, Berkeley, CA 94720-1500 USA.

D. J. Economou and V. M. Donnelly are with the Plasma Processing Laboratory, Department of Chemical and Biomolecular Engineering, University of Houston, Houston, TX 77204-4004 USA (e-mail: economou@uh.edu; vmdonnelly@uh.edu).

Color versions of one or more of the figures in this paper are available online at http://ieeexplore.ieee.org.

Digital Object Identifier 10.1109/TPS.2007.906439

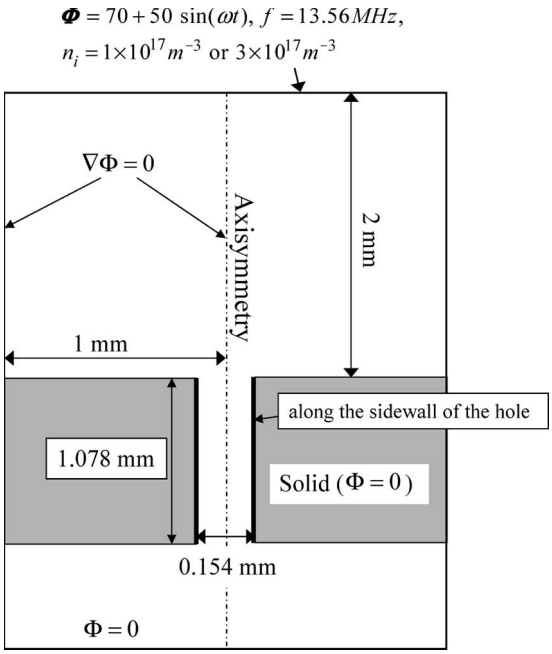

Fig. 1. Two-dimensional computational domain for neutral-beam extraction consisted of an axisymmetric hole through a solid (represented by the gray area) at ground potential, with symmetry condition in the radial direction far from the hole. The ion density, electron temperature, and plasma potential were specified at the top. Distribution functions were obtained both along the sidewall of the hole and downstream of the hole (bottom of computational domain).

In this paper, a particle-in-cell (PIC) simulation was developed to study the angular and energy distributions of a fast neutral beam extracted from a radio-frequency (RF) plasma through a grid with high-aspect-ratio holes. A single hole in contact with the plasma was considered as a simple geometry simulating a grid hole. A three-grid design to improve the extracted neutral-beam properties is also proposed.

II. Simulation Model

The 2-D axisymmetric (r, z) computational domain (see Fig. 1) extended sufficiently far above the hole to include the sheath "edge" (defined as the locus of points where the net-charge density is 1% of the local ion density). The electron temperature $(Te = 6$ eV) and RF potential $(V_0 = 70 + 50\sin(\omega t), \quad f = 13.56 \quad \text{MHz} = \omega/2\pi)$ were specified at the top boundary of the computational domain. The simulation was performed with two different ion densities at the top boundary to see the effect of different sheath thickness on plasma molding. Case 1 with $n_i = 1 \times 10^{17}$ m^{-3} and case 2 with $n_i = 3 \times 10^{17}$ m^{-3}. The thickness of the grid (wall) containing a hole was 1.078 mm, and the diameter of the hole was 0.154 mm. This gives an aspect ratio (defined as the ratio of the thickness of the grid to the diameter of the hole) of seven. The solid was conductive and at ground potential $(V = 0)$. A zero-potential gradient was applied at the perimeter boundary, and zero-potential was applied to the bottom boundary of the computational domain.

The dynamics of a collisionless plasma can be described by the Vlasov equation in 6-D phase space $(\vec{x}, \vec{\nu})$, where $\vec{x}$ and $\vec{\nu}$ are particle location and velocity, respectively

$$\frac{\partial f}{\partial t} + \vec{\nu} \cdot \frac{\partial f}{\partial \vec{x}} + \frac{\vec{F}}{m} \cdot \frac{\partial f}{\partial \vec{\nu}} = 0 \tag{1}$$

where f is the particle-distribution function, and $\overrightarrow{F} = q(\overrightarrow{E} + \overrightarrow{\nu} \times \overrightarrow{B})$ is the Lorenz force acting on a particle with charge q. The Lorenz force is generally obtained by solving Maxwell's equations. The PIC method tracks computational particles along the characteristics of the Vlasov equation with appropriate initial conditions. Particles are "pushed" according to Newton's equation of motion

$$\begin{aligned} \frac{d\vec{x}}{dt} &= \vec{\nu} \\ \frac{d\vec{\nu}}{dt} &= \frac{\overrightarrow{F}}{m}. \end{aligned} \tag{2}$$

At the end of the particle-motion time step, the charge of each particle was distributed to the nodal points of the computational mesh using bilinear interpolation. Based on the resulting charge density, Poisson's equation was solved, and the electric field was calculated on the nodal points. The electric field was then interpolated to the location of the particles using a bilinear function. The new electric field gave a new Lorentz force on the particles for the next motion time step. The cycle was repeated until a steady state was reached, and the statistics were adequate to calculate the particle-distribution functions and the potential field.

An electropositive argon plasma containing a single ion species and electrons was simulated. Only the ions were followed by the PIC simulation. The electron density was assumed to be given by the Boltzmann relation [14]. The plasma sheath evolved self-consistently according to the specified conditions. Ions at the upper boundary of the computational domain were sampled from a drifting Maxwellian distribution using the acceptance–rejection method [15]. An explicit time-centered leap-frog method [16] was used for time integration, obeying the Courant condition, $(\nu\Delta t/\Delta x) < 1$, where ν is the particle speed and Δt and Δx are the time step and grid-cell size, respectively. The pressure (5 mtorr) was sufficiently low for the ion flow to be collisionless. Particles injected at the top boundary of the computational domain were weighted according to their radial position so that a radially uniform ion flux was injected. Particle-distribution functions were collected along the sidewall of the hole (Fig. 1) and at the bottom of the computational domain. The Poisson equation was solved at each time step using a finite-element method. Time marching continued until a periodic steady state was achieved. The results shown below were obtained with 3×10^5 simulation particles. Energy conservation of the integration scheme was tested using cold $(T_i = 0)$ ions in a 2-D dc field in the domain of Fig. 1. All particles collected at the bottom of the computational domain had the same energy indicating that there were no numerical artifacts.

Ions that encountered the hole sidewall were assumed to neutralize with 100% probability [14]. Ions would neutralize by, for example, an Auger process, at a distance of the order of

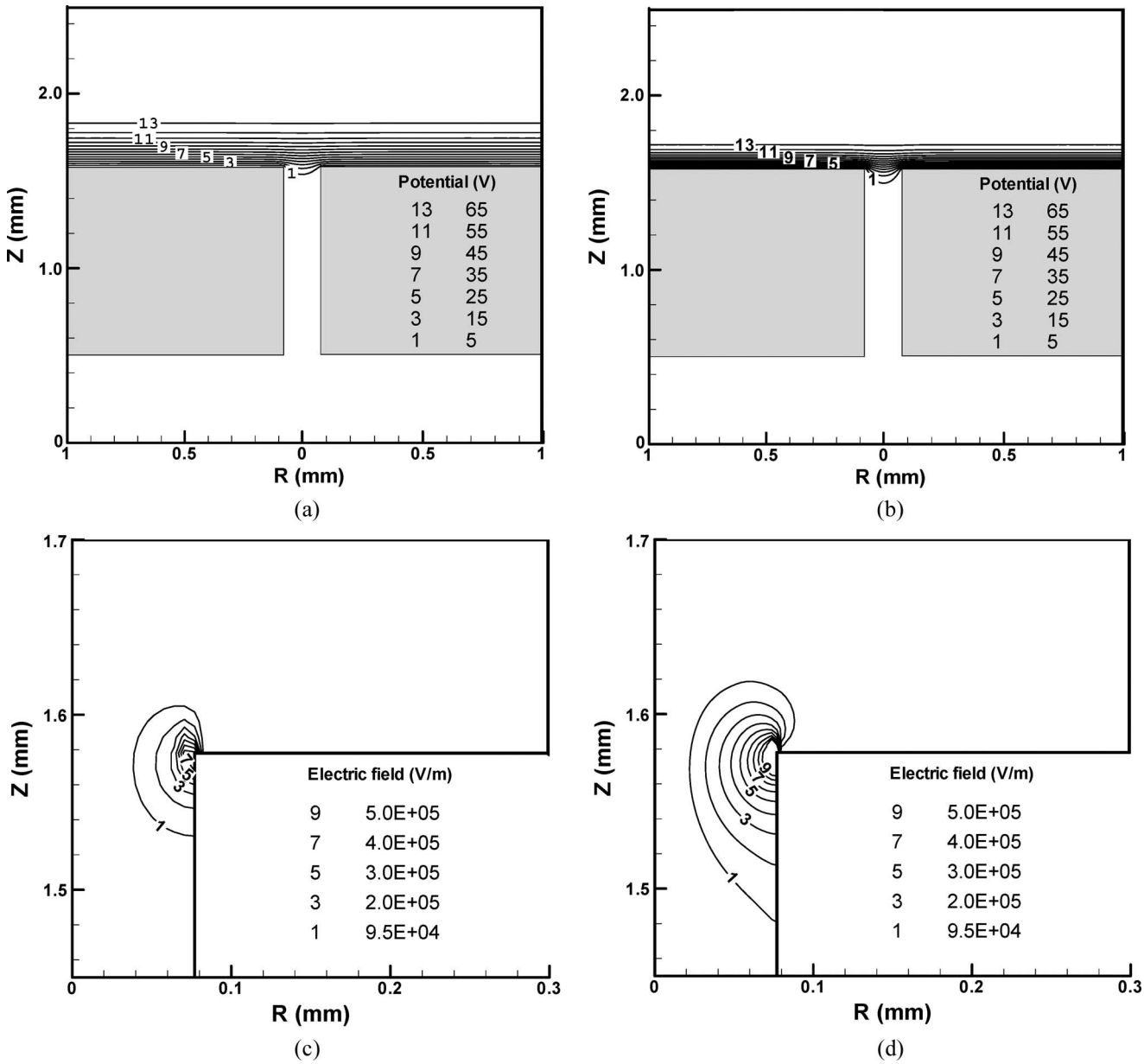

Fig. 2. Time-average potential distribution around holes with diameter of 154 μm when the ion density at the top of the domain is (a) $1 \times 10^{17}/\mathrm{m}^3$ for case 1 and (b) $3 \times 10^{17}/\mathrm{m}^3$ for case 2. Time-average horizontal component of the electric field when the ion density at the top of domain is (c) $1 \times 10^{17}/\mathrm{m}^3$ for case 1 and (d) $3 \times 10^{17}/\mathrm{m}^3$ for case 2. Ion flow was from top to bottom through the hole in a 1078-μm-thick solid grounded grid (represented by the gray area).

$\sim$1 Å from the surface. A simple surface-interaction model was used, assuming specular scattering with an energy exchange given by [17]

$$\sqrt{\frac{\varepsilon_\mathrm{r}}{\varepsilon_\mathrm{i}}} = \left(\frac{\mu}{\mu+1}\right)^2 \left(\cos\chi_{1/2} + \sqrt{\frac{1}{\mu^2} - \sin^2\chi_{1/2}}\right)^2, \qquad \chi_{1/2} = \frac{\pi}{2} - \vartheta_\mathrm{i}; \qquad \mu = \frac{\mathrm{m_{Ar}}}{\mathrm{m_{wall}}} \tag{3}$$

where ε_i and ε_r are kinetic energy of the incident and reflected atom, respectively, θ_i is the incident angle, and $\mathrm{m_{Ar}}$ and $\mathrm{m_{wall}}$ are the mass of the argon atom and the wall-material atom, respectively.

This expression corresponds to two successive binary collisions of the impinging ion (actually, a neutral by the time it encounters the surface) with surface atoms. Specular scattering may be a reasonable approximation for grazing-angle collisions with atomically flat surfaces. However, it is expected to be a poor approximation for nongrazing-angle collisions, particularly off of real (rough) surfaces.

III. Results and Discussion

A. Potential and Electric-Field Distributions

Fig. 2 shows the time-average potential distribution and the strength of the (time average) horizontal component of the electric field for the two cases studied. Case 1 ($n_i = 10^{17}/\mathrm{m}^3$) has a lower ion (and electron) density at the top boundary of the domain resulting in thicker sheath [compare Fig. 2(a)

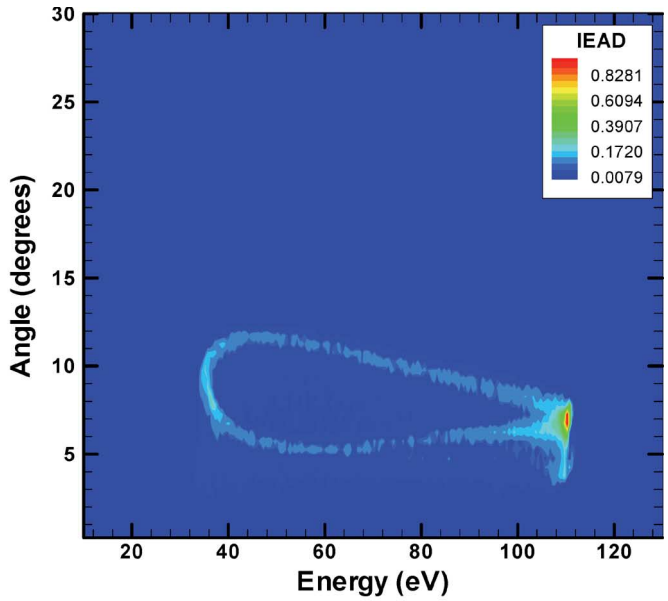

(a)

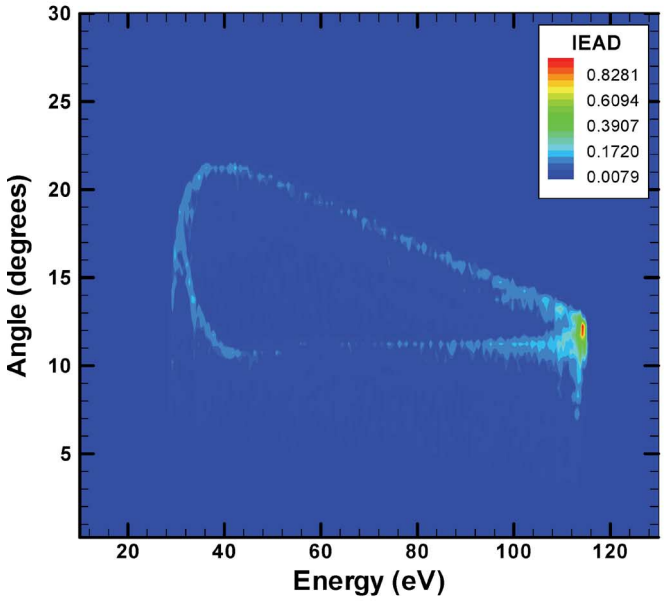

(b)

Fig. 3. IEAD all along the sidewall of the hole. (a) Case 1, $n_i = 1 \times 10^{17}/\mathrm{m}^3$. (b) Case 2, $n_i = 3 \times 10^{17}/\mathrm{m}^3$.

and (b)]. Plasma molding is less when the sheath is thicker, yielding weaker lateral electric fields [compare Fig. 2(c) and (d)]. In case 2 (more molding), ions should have more angular spread (compared to case 1) when they enter the hole due to the stronger lateral field. The different ion angular spread at the hole entrance results in different features of ions and fast neutrals inside the hole and, eventually, at the hole exit.

B. Ion and Fast Neutral-Energy-Angular Distributions (NEADs) Along the Sidewall of the Hole

Fig. 3 shows the ion energy angular distribution (IEAD) for ions impacting along the sidewall of the hole (see Fig. 1) for

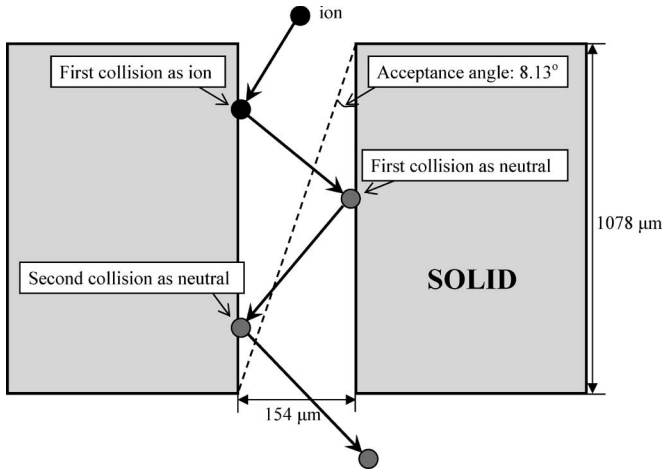

Fig. 4. Particle collisions along the sidewall of the hole and acceptance angle of the hole.

the two cases studied. In the IEAD, the x-axis is ion energy, and the y-axis is ion-incident angle. An angle of 90° implies normal incidence on the sidewall. The IEAD shows the range of angles of incidence of ions in a given energy bin. The IEAD directly affects the fast neutral-energy distribution (NED) and neutral-angular distribution (NAD), since fast neutrals are the result of ion collision with the sidewall. A range of ion energies results because the ion transit time through the sheath is a small fraction of the RF period, and ions see more or less the instantaneous sheath voltage. The IEAD for case 2 [Fig. 3(b)] exhibits larger angles and a larger range of angles as compared to case 1 [Fig. 3(a)]. This is because, for the given ion energy, more molding (thinner sheath) yields more angular spread and higher ion incidence angles. Both IEADs show that lower energy ions have more angular spread than higher energy ions, regardless of the degree of molding. A larger angle of incidence will result in more energy loss after ions collide with the wall to become neutrals.

Ions colliding with the sidewall of the hole turn into neutrals. For case 1, 94.6% of ions that entered the hole struck the wall and neutralized. The corresponding fraction for case 2 was 98%. The resulting fast neutrals can exit the hole without further collision or can collide one or more times with the sidewall (Fig. 4). This will depend on where the ion strikes the sidewall and the angle of incidence. It was found that, for the conditions of case 1, 20.9% of fast neutrals suffered only one collision with the sidewall (first collision as neutral is shown schematically in Fig. 4) and then exited the hole. The remaining 79.1% of fast neutrals exited the hole without any collision with the sidewall. The fast NEAD, for fast neutrals impacting all along the sidewall of the hole, is shown in Fig. 5, for the two cases studied. In the NEAD, the x-axis is neutral energy, and the y-axis is neutral incident angle. The NEAD of Fig. 5(a) is missing the low angle (lower half) of the corresponding IEAD of Fig. 3(a). This is because ions striking the sidewall at shallow angles turn into neutrals that exit the hole without collision. In contrast, for case 2, the NEAD of Fig. 5(b) shows a complete "ring" structure [compare to IEAD of Fig. 3(b)]. This implies that (most) neutrals suffer at least

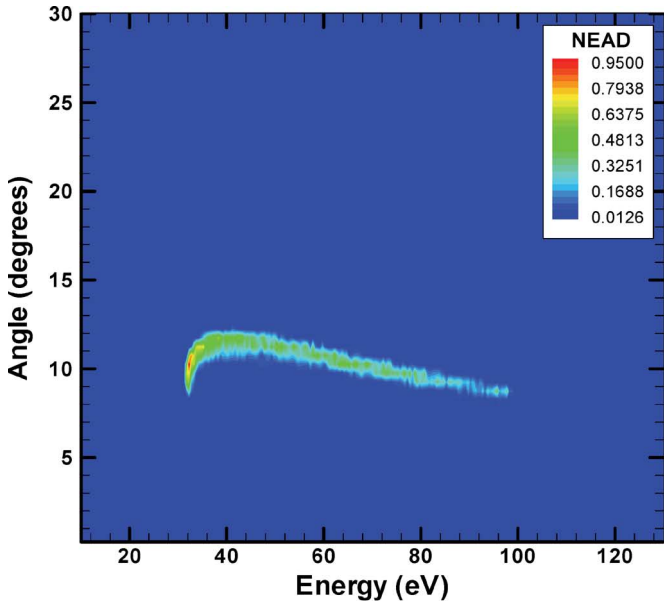

(a)

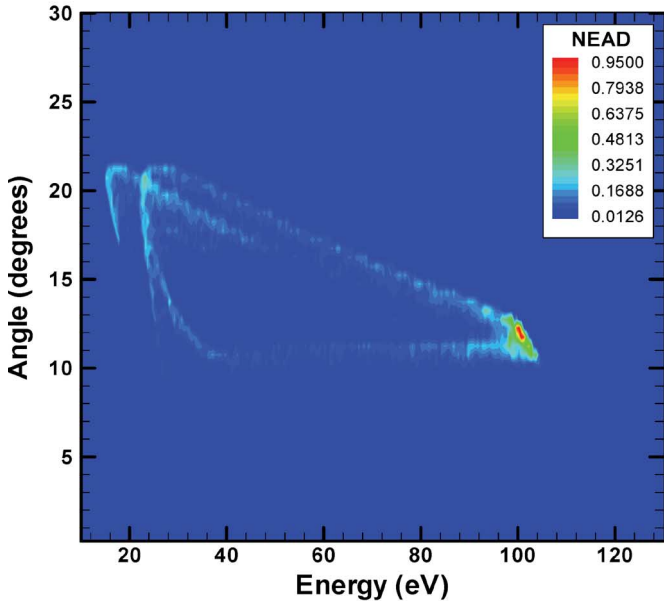

(b)

Fig. 5. Fast NEAD all along the sidewall of the hole. (a) Case 1, $n_i = 1 \times 10^{17}/\mathrm{m}^3$. (b) Case 2, $n_i = 3 \times 10^{17}/\mathrm{m}^3$.

one collision with the sidewall in this case. In fact, it was found that in case 2, 64.4% of fast neutrals suffered only one collision as neutrals, 13.8% suffered two collisions as neutrals (first collision as neutral and second collision as neutral, as shown in Fig. 4), and the remaining 21.8% of fast neutrals exited the hole without collision. The NEAD of case 2 [Fig. 5(b)] is somewhat "distorted" as compared to the corresponding IEAD [Fig. 3(b)], because ions have higher impact angles in this case (due to more severe plasma molding) and, therefore, higher energy loss. The secondary feature in the upper left corner of the NEAD of Fig. 5(b) is due to neutrals that suffer a second collision (second collision as a neutral of Fig. 4) and loose an additional amount of energy (thus shifting to the left of the plot).

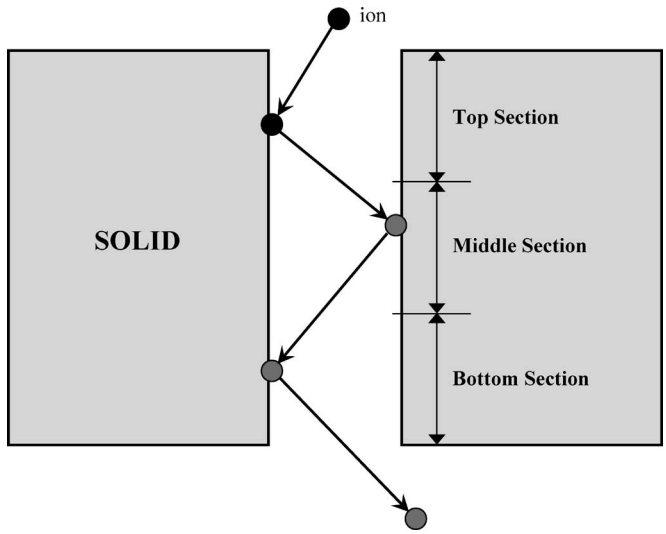

Fig. 6. Definition of top, middle, and bottom section along the sidewall of the hole.

C. Ion-Angular Distributions (IADs) at Different Locations Along the Sidewall of the Hole

IADs at different locations along the hole length are investigated in this section. The hole is divided in three equal sections as shown in Fig. 6: top, middle, and bottom sections. For cases 1 and 2, the top section is struck by ions only. No fast neutrals strike this section. In case 1 (less molding), the middle section is struck by ions only. No fast neutrals strike this section. The bottom section is struck by both ions and fast neutrals. In case 1, fast neutrals either suffer no collision or only one collision (in the bottom section) with the sidewall of the hole. In case 2, the middle section is struck by ions and fast neutrals suffering their first collision as neutrals. The bottom section is struck by ions, fast neutrals suffering their first collision as neutrals, and fast neutrals suffering their second collision as neutrals (see also Fig. 4).

Fig. 7 shows the IAD at each of the three sections of the hole. For both Fig. 7(a) and (b), the areas under the curves represent the relative number of ions striking the corresponding section. For both cases, most ions collide along the top section of the hole. Case 2 has a larger fraction of ions striking the top section of the hole due to more plasma molding. A sizeable fraction of ions collide along the top section of the hole at large angles. These ions will loose a relatively larger fraction of their energy and will be reflected at larger angles. A fraction of the resulting fast neutrals will suffer additional collision with the sidewall (perhaps more than one collision) and loose even more energy. Thus, ions that strike the top section of the hole are "bad" ions for generating high-energy and low-angular divergence neutral beams. More plasma molding will produce more of these bad ions [compare Fig. 7(a) and (b)].

D. Ion and Fast NEADs Downstream of the Hole

Fig. 8 shows the IEDs and fast NEDs downstream of the hole for cases 1 [Fig. 8(a)] and 2 [Fig. 8(b)]. The NED is shifted to lower energies as compared to the ion-energy distribution due

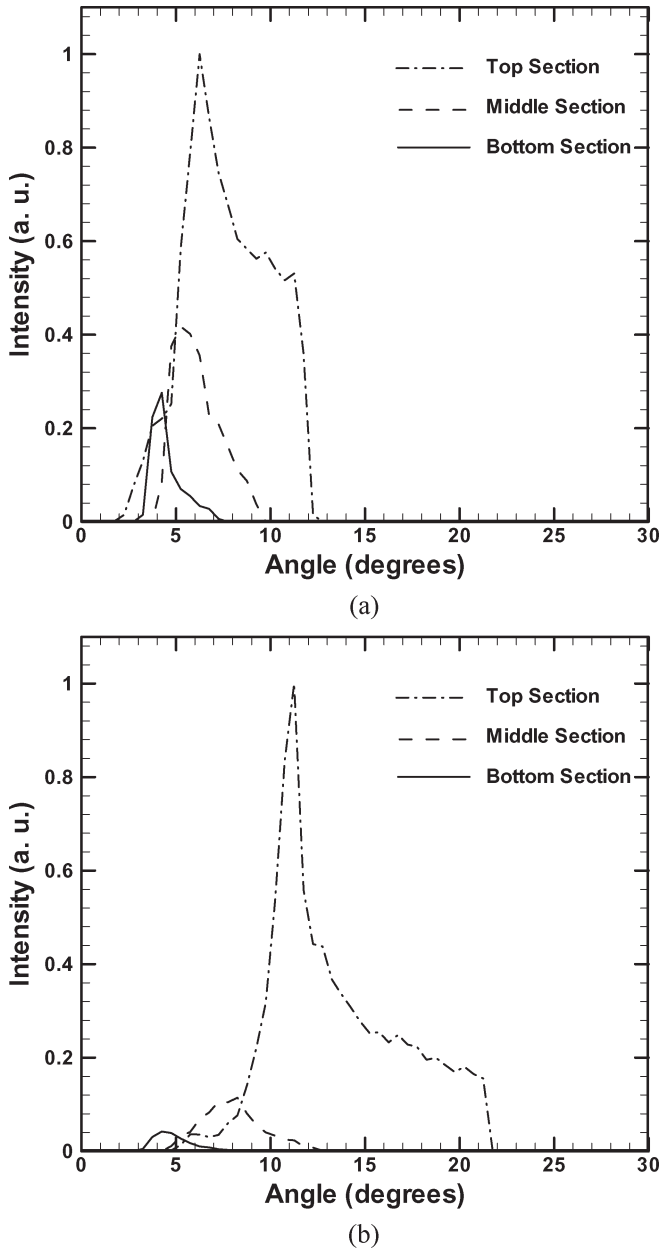

Fig. 7. IADs (normalized) on different sections of the surface of the hole. (a) Case 1, $n_i = 1 \times 10^{17}/\mathrm{m}^3$. (b) Case 2, $n_i = 3 \times 10^{17}/\mathrm{m}^3$.

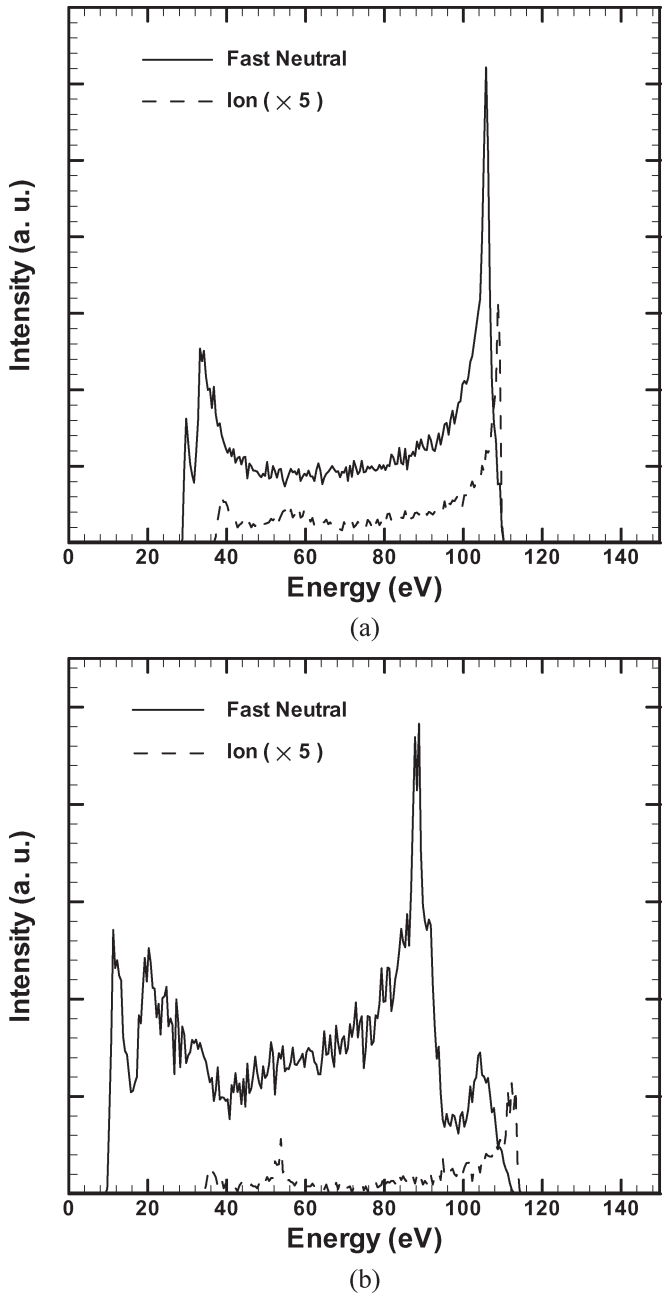

Fig. 8. IEDs and fast NEDs downstream of the hole for (a) case 1, $n_i = 1 \times 10^{17}/\mathrm{m}^3$, and (b) case 2, $n_i = 3 \times 10^{17}/\mathrm{m}^3$. Ion curves have been multiplied by five for clarity. Integral under the corresponding curves is proportional to the number of particles.

to energy loss by collision with the wall. The energy loss is given by the wall-collision model that was employed in this paper, and it is a function of the angle of incidence [see (3)]. The ion-energy-angular distribution (IEAD) along the sidewall of the hole (Fig. 3) shows that higher energy ions have smaller angle of incidence; this results in less energy shift in the high-energy region. Smaller energy ions generally collide at larger angles and loose more energy, explaining the increased energy shift in the low-energy region. The energy shifts are larger for case 2 [Fig. 8(b)], because the ion-impact angles are larger (more plasma molding). Fig. 9 shows the IADs and fast NADs downstream of the hole for cases 1 [Fig. 9(a)] and 2 [Fig. 9(b)]. The integral under the respective curves is proportional to the total number of ions and fast neutrals exiting the hole. The IAD cannot exceed about 8°, which is the acceptance angle of the hole (see Fig. 4). The NAD has a "hole" at small angles, because fast neutrals are generated only by specular reflection of ions striking the wall. Vertical or small angle ions do not strike the wall and cannot generate fast neutrals. Case 2 yields more divergent fast neutrals of wider angular distribution as compared to case 1, again due to more plasma molding. In fact, the fast NADs at the exit of the hole resemble the IADs on the hole sidewall (Fig. 7). Comparison between Figs. 7 and 9 shows that most fast neutrals are generated by ions striking the top section of the hole.

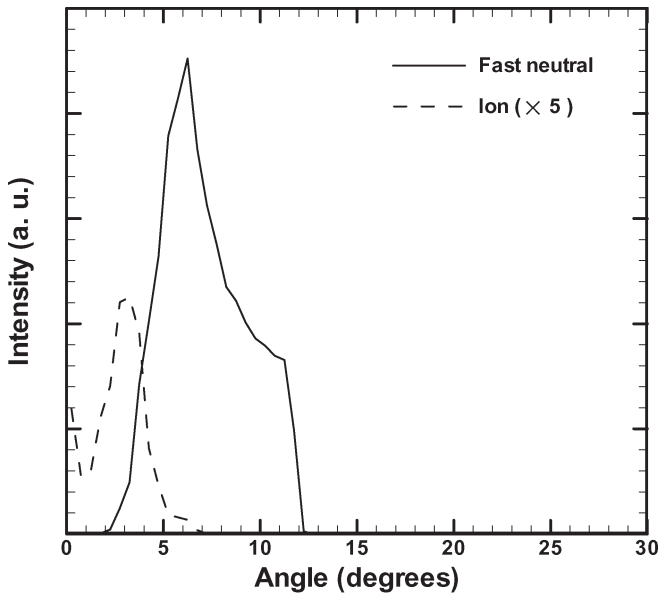

(a)

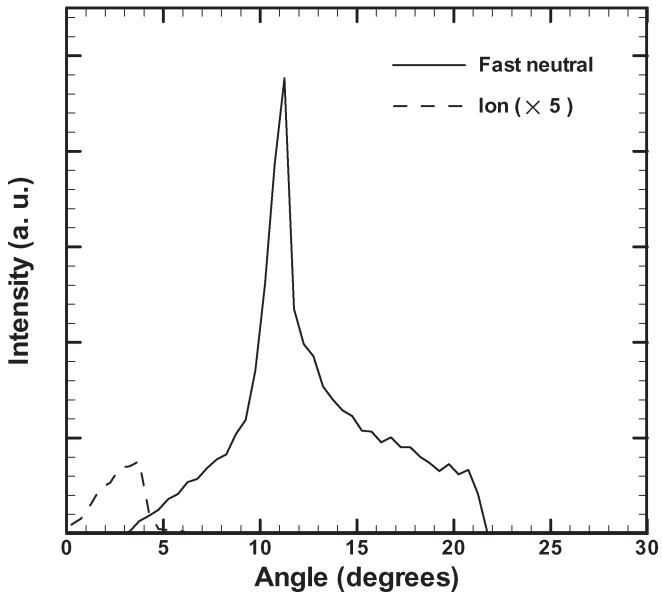

(b)

Fig. 9. IADs and fast NADs downstream of the hole for (a) case 1, $n_i = 1 \times 10^{17}/\mathrm{m}^3$, and (b) case 2, $n_i = 3 \times 10^{17}/\mathrm{m}^3$. Ion curves have been multiplied by five for clarity. Integral under the corresponding curves is proportional to the number of particles.

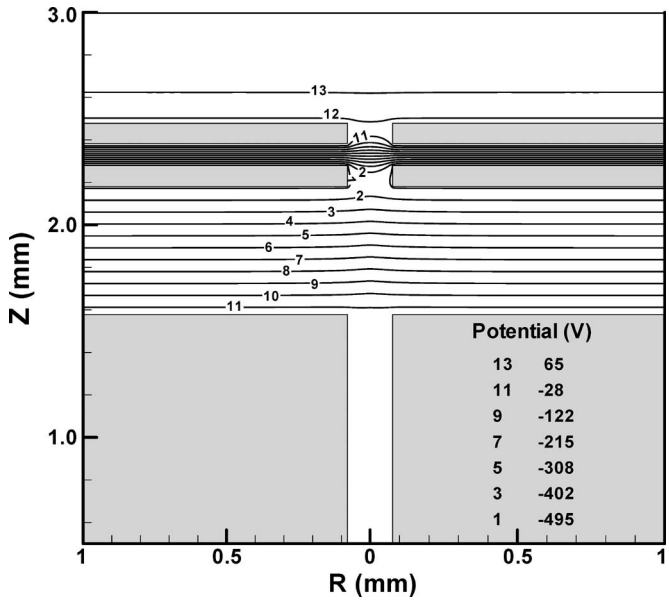

Fig. 10. Potential distribution in the three-grid system. Grids are shown in gray shading. The top grid (in contact with plasma) is 100 μm thick and is kept at ground potential. The middle grid (also 100 μm thick) is biased at -500 V. The bottom grid is 1078 μm thick and is kept at ground potential. The spacing between the top two grids is 100 μm. A hole, 158 μm in diameter, runs through the grids. Most ions extracted from the plasma neutralize by collision with the sidewall of the high-aspect-ratio hole of the bottom grid. Other conditions were as in Fig. 1 with $n_i = 3 \times 10^{17}/\mathrm{m}^3$ (case 2).

E. Three-Grid Ion-Extraction/Neutralization System

The above analysis reveals that too much plasma molding is not desirable since ions are severely deflected, resulting in divergent neutral beams with lower energy. In order to minimize plasma molding in the one-grid system studied so far, one must assure that the sheath thickness is considerably larger than the hole diameter. This can be accomplished either by increasing the sheath thickness or by decreasing the hole diameter (or both). The former can be achieved by lowering the plasma density, which, however, lowers the overall processing rate. On the other hand, a grid with very small-diameter high-aspect-ratio holes may be difficult to fabricate. A way to minimize plasma molding while simultaneously keeping a reasonable hole diameter and high plasma density is a three-grid system (Fig. 10). The top-grounded grid is in contact with the plasma. The middle grid is biased with a high negative-dc potential (-500 V in the present case). The bottom grid, with high-aspect-ratio holes, is also grounded. In a single-grid system, the plasma sheath would tend to "dip" inside the hole. The purpose of the middle grid is to "repel" the sheath back into the plasma. Depending on the strength of the applied negative potential, the sheath may be made to dip into the hole, be flat, or bulge back into the plasma. The purpose of the top grid is to shield the potential applied to the middle grid. The purpose of the bottom grid is to neutralize the extracted ions by collision with the sidewall of the high-aspect-ratio hole.

The time-average potential profile in the three-grid system is shown in Fig. 10 for a -500-V dc applied to the middle grid (only part of the computational domain is shown for clarity). The plasma parameters were as in Fig. 1, with $n_i = 3 \times 10^{17}/\mathrm{m}^3$ (case 2). The three-grid system acts as a lens where the plasma sheath is an additional "virtual" electrode. The ion energy is still equal to the plasma potential (as in the one-grid system), since ions still travel from the plasma to the grounded bottom grid surface. Due to the lens action, positive ions do not strike the negatively biased grid for the conditions employed. Ions are extracted by the top grids and are neutralized by wall collisions on the bottom grid. The energy and angular distributions of ions and fast neutrals at the downstream of the hole are shown in Fig. 11 for case 2 ($n_i = 3 \times 10^{17}/\mathrm{m}^3$). The energy distributions [Fig. 11(a)] for both ions and fast neutrals have a larger fraction of higher

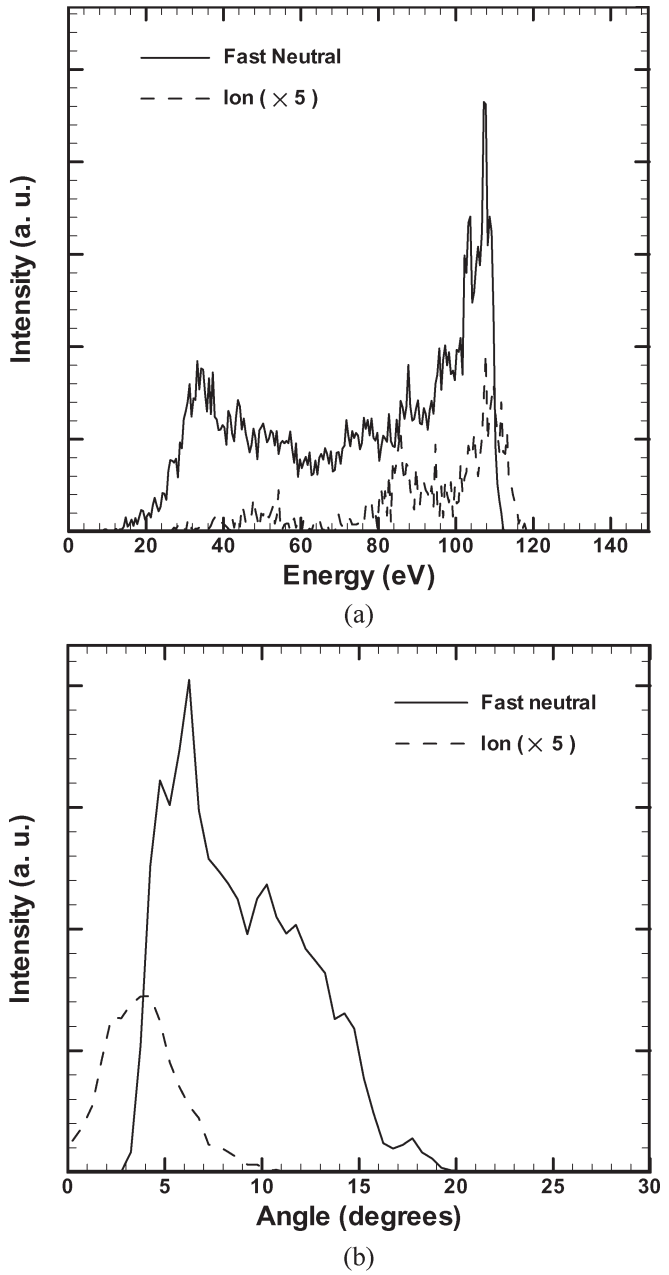

Fig. 11. Ion and fast (a) NED and (b) NAD at the hole exit for the three-grid system and $n_i = 3 \times 10^{17}/\mathrm{m}^3$ (case 2). Ion curves have been multiplied by five for clarity. Integral under the corresponding curves is proportional to the number of particles.

energy particles (compare to Fig. 8(b), which is for the one-grid system for case 2). The angular distributions [Fig. 11(b)] are even more revealing, showing a much larger fraction of lower angle fast neutrals as compared to the one-grid system [Fig. 9(b)]. This can be better understood by looking at the angular distributions of ions impacting the three equal sections of the hole of the bottom grid (Fig. 12). A much larger fraction of "good" ions (smaller angles of impact or more grazing-angle collisions) is generated by the three-grid system as compared to the one-grid case shown earlier [Fig. 7(b)]. In the three-grid system, an appreciable fraction of ions that impinge on the top section of the high-aspect-ratio hole are good (angular diverge of only a few degrees), in contrast to the one-grid system.

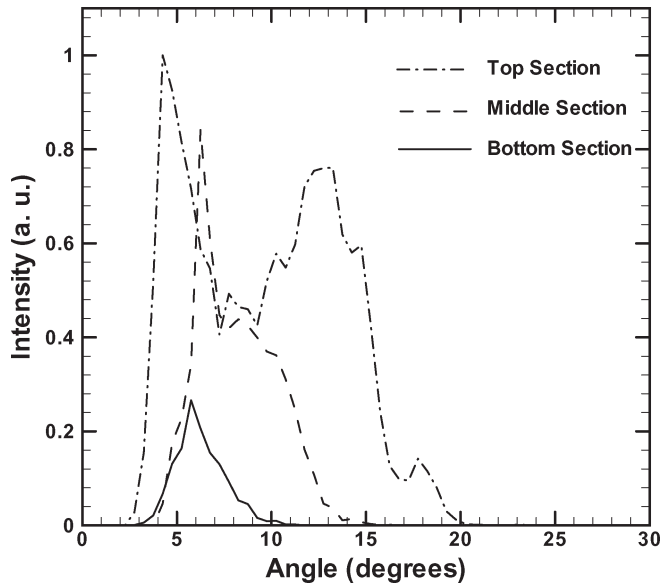

Fig. 12. IAD along the three sections of the high-aspect-ratio hole of the three-grid system and $n_i = 3 \times 10^{17}/\mathrm{m}^3$ (case 2). Integral under the corresponding curves is proportional to the number of particles.

If one defines good ions as ions that strike the sidewall of the high-aspect-ratio hole at angles less than the acceptance angle (Fig. 4), then, for case 2, the fraction of good ions for the one-grid system was 9% while that for the three-grid system was 46%. The fraction of good ions for case 1 was 65%, since case 1 had less plasma molding, corresponding to less ion-trajectory distortion, and a larger fraction of ions colliding with the hole sidewall at grazing angles. Finally, the degree of ion neutralization (fraction of ions that enter the hole, which suffer a collision and neutralize) was 95.2% for the three-grid system, comparable to cases 1 and 2 of the one-grid system.

IV. Conclusion

A PIC simulation was developed to study the effect of plasma molding on the energy and angular distributions of ion and fast neutral beams extracted from a hole in contact with a high density plasma. Plasma molding refers to "distortion" of the plasma sheath over surface topography. Such distorted sheath can divert an otherwise collimated ion beam, increasing the angular spread of the beam. Emphasis was placed on ion neutralization by collision with the internal surface of high-aspect-ratio holes. This is one method of generating a fast neutral beam that can find applications in charge-free microelectronics manufacturing. When the sheath thickness is much smaller than the diameter of the hole, plasma molding is severe, the plasma-sheath interface "dips" inside the hole, and the resulting ion and neutral beams are highly divergent. When the sheath thickness is much larger than the hole diameter, plasma molding is weak and collimated beams may be extracted. The angular distribution of fast neutrals peaks off axis. The fast NED is similar to that of ions but is shifted to lower energies as ions loose energy in collisions with the wall.

The IEAD, for ions striking the sidewall of the hole, indicated that ions with lower energy tend to be affected more by plasma

molding, resulting in larger angles of incidence on the sidewall. The energy and angular distributions of ions and fast neutrals at the bottom section of the hole sidewall were not affected as much by plasma molding. In contrast, plasma molding affected the distributions of ions and fast neutrals striking the top section of the hole sidewall. In general, ions that neutralized on the top section of the hole sidewall were "bad," in the sense that these ions yielded divergent neutral beams of relatively low energy. Ions that neutralized along the bottom section of the hole sidewall were "good," in the sense that these ions yielded neutral beams that were less divergent and retained more of the energy of the parent ions.

A three-grid ion-extraction/neutralization system was proposed to increase the fraction of good ions in cases of excessive plasma molding and improve the quality of the extracted fast neutral beam. This system allowed plasma molding to be controlled, even for high plasma densities and large hole diameters, when plasma molding for a one-grid system would be severe.

ACKNOWLEDGMENT

S. K. Nam would like to thank Prof. J. P. Verboncoeur of UC Berkeley for useful exchanges regarding PIC.

REFERENCES

[1] J. Matsui, N. Nakano, Z. L. Petrovic, and T. Makabe, "The effect of topographical local charging on the etching of deep-submicron structures in SiO_2 as a function of aspect ratio," *Appl. Phys. Lett.*, vol. 78, no. 7, pp. 883–885, Feb. 2001.

[2] D. J. Economou and R. C. Alkire, "Effect of potential field on ion deflection and shape evolution of trenches during plasma-assisted etching," *J. Electrochem. Soc.*, vol. 135, no. 4, pp. 941–949, Apr. 1988.

[3] S. Samukawa, Y. Minemura, and S. Fukuda, "Control of nitrogen depth profile in ultrathin oxynitride films formed by pulse–time-modulated nitrogen beams," *J. Vac. Sci. Technol. A, Vac. Surf. Films*, vol. 22, no. 2, pp. 245–249, Mar. 2004.

[4] S. Panda, D. J. Economou, and L. Chen, "Anisotropic etching of polymer files by high energy ($\sim$100 s of eV) oxygen atom neutral beams," *J. Vac. Sci. Technol. A, Vac. Surf. Films*, vol. 19, no. 2, pp. 398–404, Mar. 2001.

[5] S. Samukawa, K. Sakamoto, and K. Ichiki, "Generating high-efficiency neutral beams by using negative ions in an inductively coupled plasma source," *J. Vac. Sci. Technol. A, Vac. Surf. Films*, vol. 20, no. 5, pp. 1566–1573, Sep. 2002.

[6] H. Kuwano and F. Shimokawa, "Silicon dioxide fine patterning by reactive fast atom beam etching," *J. Vac. Sci. Technol. B, Microelectron. Process. Phenom.*, vol. 6, no. 5, pp. 1565–1569, Sep. 1988.

[7] C. A. Nichols and D. M. Manos, "Simulation of a surface-reflection neutral stream source," *J. Appl. Phys.*, vol. 80, no. 5, pp. 2643–2649, Sep. 1996.

[8] J. W. Cuthbertson, R. W. Motley, and W. D. Langer, "High-flux source of low-energy neutral beams using reflection of ions from metals," *Rev. Sci. Instrum.*, vol. 63, no. 11, pp. 5279–5288, Nov. 1992.

[9] S. J. Kim, H. J. Lee, G. Y. Yeom, and J. K. Lee, "Requirements of neutral beam source regarding gas pressure and neutral angle for nanoscale etching," *Jpn. J. Appl. Phys.*, vol. 43, no. 10, pp. 7261–7266, 2004.

[10] S. M., Rossnagel, J. J. Cuomo, and W. D. Westwood, Eds., *Handbook of Plasma Processing Technology*. Park Ridge, NJ: Noyes, 1990.

[11] D. Kim and D. J. Economou, "Plasma molding over surface topography: Simulation of ion flow, and energy and angular distributions over steps in RF high-density plasmas," *IEEE Trans. Plasma Sci.*, vol. 30, no. 5, pp. 2048–2058, Oct. 2002.

[12] C.-K. Kim and D. J. Economou, "Plasma molding over surface topography: Energy and angular distribution of ions extracted out of large holes," *J. Appl. Phys.*, vol. 91, no. 5, pp. 2594–2603, Mar. 2002.

[13] S. K. Nam, D. J. Economou, and V. M. Donnelly, "Particle-in-cell simulation of beam extraction through a hole in contact with plasma," *J. Phys. D, Appl. Phys.*, vol. 39, no. 18, pp. 3994–4000, Sep. 2006.

[14] M. A. Lieberman and A. J. Lichtenberg, *Principles of Plasma Discharges and Materials Processing*. New York: Wiley, 1994.

[15] G. A. Bird, *Molecular Gas Dynamics and the Direct Simulation of Gas Flows*. Oxford, U. K.: Clarendon, 1994.

[16] C. K. Birdsall, "Particle-in-cell charged-particle simulations, plus Monte Carlo collisions with neutral atoms, PIC–MCC," *IEEE Trans. Plasma Sci.*, vol. 19, no. 2, pp. 65–85, Apr. 1991.

[17] B. A. Helmer and D. B. Graves, "Molecular dynamics simulations of Ar^+ and Cl^+ impacts onto silicon surfaces: Distributions of reflected energies and angles," *J. Vac. Sci. Technol. A, Vac. Surf. Films*, vol. 16, no. 6, pp. 3502–3514, Nov. 1998.

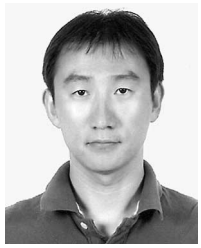

Sang Ki Nam received the Ph.D. degree in chemical engineering from the University of Houston, Houston, TX, in 2006.

He was with the Plasma Processing Laboratory, Department of Chemical and Biomolecular Engineering, University of Houston. He is currently a Postdoctoral Associate with the Department of Nuclear Engineering, University of California, Berkeley, Berkeley, working on the simulation of the high-power microwave system, using the particle-in-cell simulation method. His research interests include fluid and particle simulation of plasmas, ion and neutral beam sources, nanopantography, and microplasmas.

Demetre J. Economou received the Ph.D. degree in chemical engineering from the University of Illinois, Urbana-Champaign, in 1986.

Since 1986, he has been with the Department of Chemical and Biomolecular Engineering, University of Houston, Houston, TX, where he is currently a John and Rebecca Moores Professor and the Associate Chairman. His research interests include plasma modeling and simulation, plasma diagnostics, microplasmas, nanopantography, and neutral beam sources. He is the author or coauthor of almost 150 scientific articles and book chapters in these areas. He has organized several international symposia and has made nearly 200 technical presentations in conferences, industry, and academia, including 60 invited talks.

Dr. Economou is a Fellow of the American Vacuum Society. In addition to this Special Issue, he has served as a Guest Editor of Special Issues of the IEEE TRANSACTIONS ON PLASMA SCIENCE on the modeling of low-temperature plasmas published in August 1995, October 1999, and August 2003.

Vincent M. Donnelly received the B.A. degree in chemistry from LaSalle University, Philadelphia, PA, in 1972 and the Ph.D. degree in physical chemistry from the University of Pittsburgh, Pittsburgh, PA, in 1977.

He joined Bell Telephone Laboratories in 1979; after two years, he joined the Naval Research Laboratory, Washington DC, as a National Research Council Postdoctoral Fellow. He was with Bell Laboratories, Lucent Technologies, Murray Hill, NJ, as a Distinguished Member of the Technical Staff. Since 2002, he has been with the Plasma Processing Laboratory, Department of Chemical and Biomolecular Engineering, University of Houston, Houston, TX, in 2002, as a Professor. He has published more than 160 papers and has given more than 100 invited talks. He is the holder of ten patents. His research interests include new nanopatterning methods, experimental studies of plasma etching, optical diagnostic techniques for processing plasmas, plasma-surface chemistry, and atmospheric pressure microplasmas.

Dr. Donnelly received the Tegal Corporation Thinker's Award in 1991 and the AVS Plasma Science and Technology Division Plasma Prize in 2003.